



Electrochemical growth of a corrosion-resistant multi-layer scale to enable an oxygen-evolution inert anode in molten carbonate

Diyong Tang^a, Kaiyuan Zheng^a, Huayi Yin^{a, b, **}, Xuhui Mao^a, Donald R. Sadoway^b, Dihua Wang^{a, *}

^a School of Resource and Environmental Sciences, Hubei International Scientific and Technological Cooperation Base of Sustainable Resource and Energy, Wuhan University, Wuhan, 430072, PR China

^b Department of Materials Science and Engineering, Massachusetts Institute of Technology, Cambridge, 02139, MA, USA

ARTICLE INFO

Article history:

Received 8 January 2018

Received in revised form

11 March 2018

Accepted 14 May 2018

Available online 21 May 2018

Keywords:

Nickel alloy

Anodic oxidation

Molten salt

High-temperature electrochemistry

Inert anode

ABSTRACT

An *in-situ* formed three-layered scale consisting of a Cu-rich layer and two oxide layers on the surface of Ni₁₀Cu₁₁Fe alloy enables an inert anode for oxygen evolution reaction in molten Na₂CO₃-K₂CO₃. The outermost layer is mostly NiFe₂O₄, the middle layer mainly consists of NiO, and the innermost is a Cu-rich metal layer. The dense NiFe₂O₄ layer is resistant to molten salts and prevents O²⁻ diffusing inwards, the middle NiO layer conducts electrons and functions as a buffer layer to increase the mechanical robustness of the whole scale, and the third copper-rich layer could help to slow down the oxidation rate of the alloy. This low-cost inert anode with a multi-layered scale is able to survive for more than 600 h in molten Na₂CO₃-K₂CO₃ electrolysis cell, generating O₂ and thereby enabling a carbon-free electro-metallurgical process.

© 2018 Elsevier Ltd. All rights reserved.

1. Introduction

With the exception of noble metals (e.g., Au, Pt, Ir, etc.), a corrosion-resistant oxide layer is requisite for pure metals and alloys surviving as an anode in a high-temperature atmosphere or oxide-ion containing molten salts. Low-cost transition-metal alloys have been considered as promising inter anode candidates in molten-salt electrolysis cells, such as Hall-Héroult [1,2], FFC Cambridge [3–5], molten oxide electrolysis [6–8], molten carbonate electrolysis [9–12]. The vector of electrochemical metallurgy points towards green process development featuring low energy consumption and zero-emissions. Therefore, a low-cost inert anode is key to accomplishing an environmentally sound electrolysis process, without producing CO₂ and toxic byproducts, but generating oxygen.

In addition to the widely used molten halide electrolytes in the current electrolysis industry, molten carbonate has been in the past

few years found to be an electrolyte capable of producing iron, nickel, and cobalt and oxygen with a low-cost Ni₁₀Cu₁₁Fe inert anode [10–12]. Unlike molten halide electrolytes, molten carbonate has a narrow electrochemical window but less corrosivity. Besides ceramics and cermets, metallic inert anodes are promising candidates due to their low cost, high electronic conductivity, ease of fabrication, excellent thermal shock resistance, and mechanical robustness [13]. Amongst the metallic inert anodes, the nickel-based alloys have been intensively studied due to their low cost, mechanical robustness and formation of a nickel ferrite coating [14–23]. Generally, transition metals and their alloys can be oxidized prior to the oxygen evolution because of their lower electronegativity than oxygen. In order to make the low-cost transition metallic alloys work as inert anodes, a dense and electrically conductive oxide layer on the surface of the alloys should be constructed to protect the bulk metal anode and subsequently enable oxygen evolution [24]. After the electrically conductive oxide layer forms, the oxygen evolution reaction takes place at the interface of the oxide layer and electrolyte, providing electrons to the metallic anode underneath the oxide layer, and then the electrons are transferred through the external circuit to the cathode for reduction reactions. Therefore, constructing a dense and stable protective oxide layer, while maintaining its electrical conductivity,

* Corresponding author. School of Resource and Environmental Sciences, Wuhan University, Wuhan, 430072, PR China.

** Corresponding author. Department of Materials Science and Engineering, Massachusetts Institute of Technology, MA, 02139, USA.

E-mail addresses: huayi@mit.edu (H. Yin), wangdh@whu.edu.cn (D. Wang).

oxygen catalytic activity, mechanical robustness and an appropriate thickness, is crucial to the success of the metallic inert anode.

Direct electrochemical formation of a functionally protective oxide scale on the surface of alloys is a straightforward approach, taking advantage of electrochemical corrosion of metal anode in a short term and thereby enabling a long-term stability. Herein, the electrochemical growth of the protective oxide scale and its structure are studied to reveal the oxide growth process and structures, which allows us to have a better understanding of the electrochemical corrosion mechanism of Ni10Cu11Fe in molten carbonate, and thereby inspiring future inert anode development.

2. Materials and methods

2.1. Materials and experimental setup

Ni10Cu11Fe anode was fabricated by casting the mixed nickel, copper and iron powders (79:10:11 in mass ratio, analytical purity (>99.9%), Sinopharm Chemical Reagent Co. Ltd., China) in an alumina crucible (20 mm in inner diameter) protected in an Ar atmosphere at 1600 °C, and the alumina crucible was heated by a MoSi₂ pole furnace. A porous Fe₂O₃ pellet was attached to an iron wire (2 mm in diameter) working as a cathode, and the as-prepared Ni10Cu11Fe was employed as an anode for electrolysis [10]. The electrolysis cell was contained in an alumina crucible containing 500 g anhydrous Na₂CO₃-K₂CO₃ (59:41 in molar ratio, analytical purity (>99.9%), Sinopharm Chemical Reagent Co. Ltd., China), and the salt was dried in air at 250 °C for 48 h in a closed-end sealed stainless steel (SS) reactor. Then the temperature of the SS reactor was raised to 750 °C to melt the salt with the protection of Ar flow. Pre-electrolysis was performed under a constant cell voltage of 1.8 V between a Ni10Cu11Fe alloy anode and a foamed nickel cathode for 2 h to further remove residual water and, if any, other impurities from the molten salts.

2.2. Electrochemical measurements

Cyclic voltammetry (CV) measurements were conducted in a three-electrode setup controlled by a CHI1140a electrochemical workstation (Shanghai Chenhua Instrument Co. Ltd., China). Nickel, iron, copper, platinum wires (1 mm in diameter, Alfa Aesar), and Ni10Cu11Fe alloy were respectively employed as a working electrodes, with a graphite rod (6 mm in diameter) counter electrode and a Ag/Ag₂SO₄ reference electrode. The onset potential begins at open circuit potential (OCP). The reference electrode was made by inserting a silver wire (2 mm in diameter) into a eutectic carbonate melt (Li₂CO₃:Na₂CO₃:K₂CO₃ = 43.5: 31.5: 25 mol %) containing Ag₂SO₄ (0.1 mol/kg) in a mullite cylinder. Electrochemical impedance spectroscopy (EIS) tests were conducted to test the conductivity of the formed oxides coating of Ni10Cu11Fe anode by an electrochemical workstation (Autolab 302 N, Metrohm), and the excitation ac signal with amplitude of 5 mV in a frequency domain from 1 Hz to 10 kHz was applied and the DC potential was controlled at the open circuit potential. The Ni10Cu11Fe rod served as working electrode, an iron sheet (3 cm × 4 cm) was used as a counter electrode, and the Ag/Ag₂SO₄ was the reference electrode. All experiments were performed under the protection of high purity argon flow (>99.999%).

2.3. Oxide scale formation and characterization

A two-electrode electrolysis cell consisting of a sintered Fe₂O₃ pellet cathode, the casted Ni10Cu11Fe anode, and a molten Na₂CO₃-K₂CO₃ electrolyte was assembled in the SS test vessel to *in-situ* form an oxide scale and test the stability of the inert anode covered with

the oxide scale. The electrolysis cell was operated under constant cell voltage and controlled by a battery testing system (Shenzhen Neware Electronic Ltd., China). After the Fe₂O₃ pellet cathode was completely reduced to Fe, new Fe₂O₃ pellets were refilled at regular intervals to supply O²⁻ and enable the anode to work under certain current densities with the same electrolyte and anode. The resistance of the anode under different electrolysis durations was measured by EIS. After electrolysis, the grown protective layer on the surface of the anode was cross-sectioned and analyzed by scanning electron microscopy (SEM, FEI Sirion field emission, including second and backscattered electron imaging), X-ray diffraction spectroscopy (XRD, Shimadzu X-ray 6000 with Cu K α 1 radiation at $\lambda = 1.5405 \text{ \AA}$) and energy-dispersive X-ray spectroscopy (EDX, EDAX GENESIS 7000). The outlet gas from the electrolysis chamber was analyzed by gas chromatography (GC) (Shanghai Kechuang).

3. Results and discussion

3.1. Thermodynamic analysis

The theoretical electrochemical window of molten Na₂CO₃-K₂CO₃ is 2.34 V at 750 °C, and the anodic and cathodic limit reactions are oxygen evolution and sodium deposition, respectively. If an inert anode was made of noble metal, like platinum, is employed, oxygen can be generated at the anode. Thermodynamic data of the molten carbonate system were analyzed in detail by Van et al. [25]. Thermodynamically, the transition-metal will be oxidized in molten carbonate under anodic polarization. The Gibbs free energy of the anodic reactions of Ni, Fe and Cu in molten Na₂CO₃-K₂CO₃ was obtained from *HSC Chemistry 6*. The standard dissociation potentials of the reactions are calculated from the Nernst equation ($\Delta G = -nFE$, the chemical activity of all species is assigned as unity, n is the number of transferred electrons, and F is the Faraday constant). As shown in Fig. 1, the oxides scale could form on the surface of Ni, Fe and Cu electrodes prior to oxygen evolution. Among these three metals, iron oxides preferentially form, then nickel oxide forms, and copper oxides form lastly. At the very beginning of electrolysis, the electrochemical oxidation of anode takes place at the alloy/electrolyte interface. Afterwards, the oxides grow at alloy/oxides interface, and simultaneously compounding reactions could occur inside the oxide scale and further oxidation could give rise to the formation of the spinel NiFe₂O₄ at the scale/metal interface. There are two kinds of reactions taking place spontaneously. One reaction is named a displacement

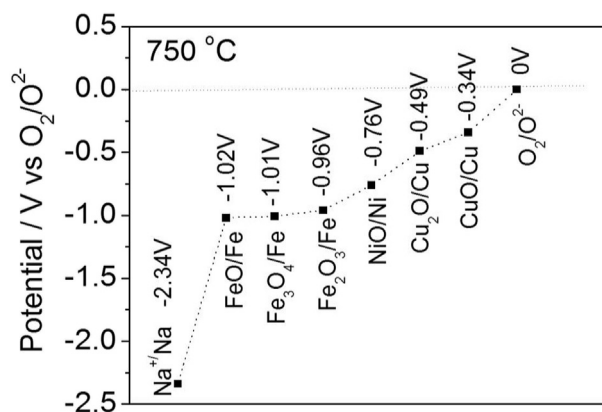


Fig. 1. Standard potentials of the half reactions versus oxygen evolution potential at 750 °C, all thermodynamic data are obtained from HSC Chemistry 6.

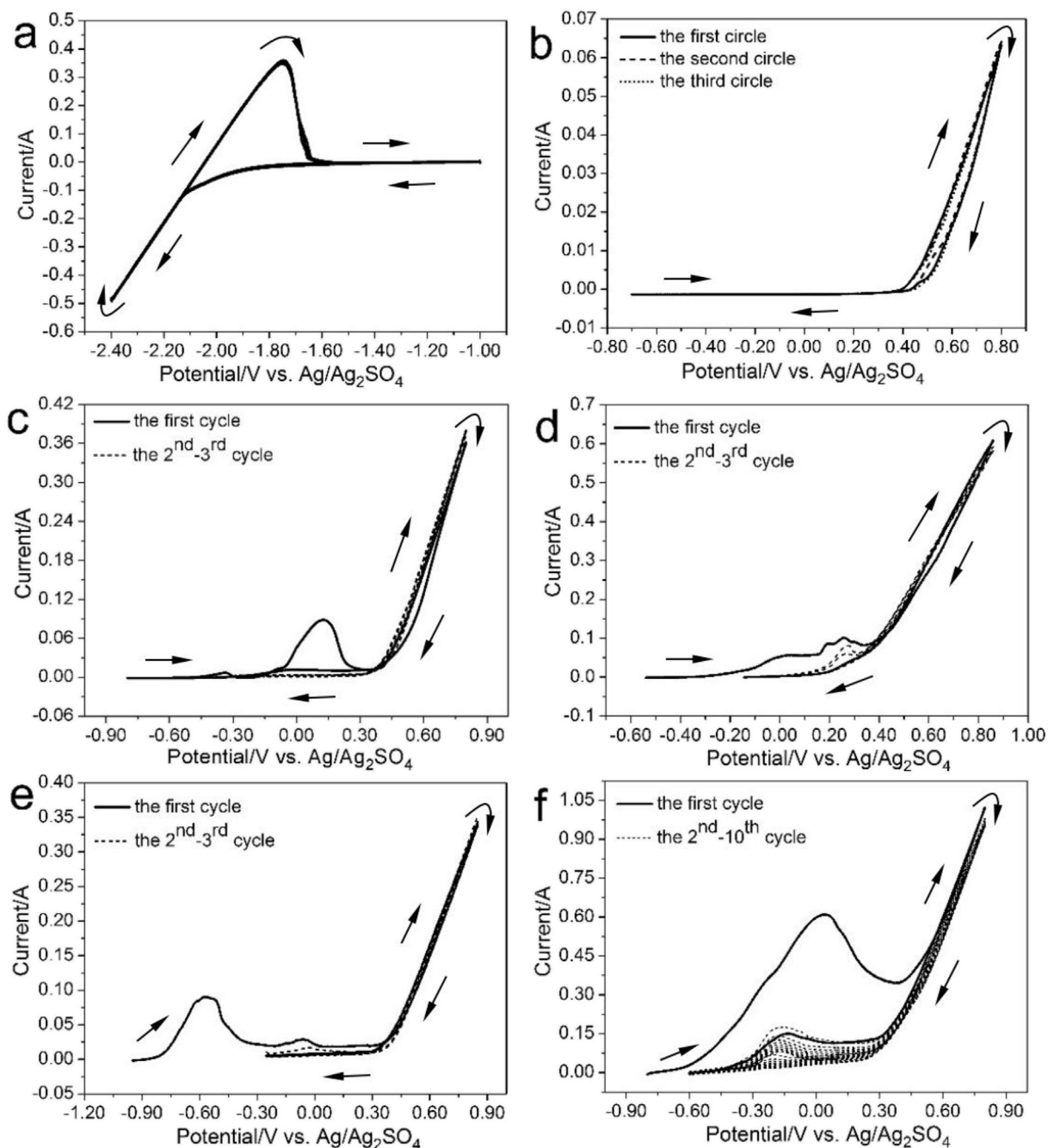


Fig. 2. Cyclic voltammograms of the iron (a), platinum (b), nickel (c), copper (d), iron (e) wires, and Ni10Cu11Fe rod (f) in $\text{Na}_2\text{CO}_3\text{-K}_2\text{CO}_3$ eutectic melt at 750°C . Scan rate: 2 mV/s.

reaction: for example, the Fe can displace Ni and Cu from NiO and $\text{Cu}_2\text{O}/\text{CuO}$, and Ni and Fe can displace Cu from copper oxides while generating iron- and nickel-oxides. Another reaction happening inside the oxide layer is called compounding reaction, such as Fe_2O_3 reacting with NiO to form NiFe_2O_4 . Note that, the displacement does not contribute to the growth of the oxide scale. To achieve a long-lasting metal anode, these two kinds of reactions should stop when a protective layer reaches a proper thickness. Otherwise the oxide layer will continuously grow and the monolithic body of the alloy anode will be oxidized completely in the end. Therefore, the structure and component of the protective layer are crucial to maintain the stability and functionality of the inert anode.

3.2. Electrochemical behaviors of the metal electrodes

The anodic behaviors of Ni, Fe, Cu, Ni10Cu11Fe alloy, and Pt were investigated by cyclic voltammetry to study their electrochemical oxidation processes. In molten $\text{Na}_2\text{CO}_3\text{-K}_2\text{CO}_3$ electrolyte, the cathodic limit on the pure iron working electrode is -2.0 V (Fig. 2a) (unless otherwise noted, all potentials mentioned in this paper refer to the $\text{Ag}/\text{Ag}_2\text{SO}_4$ reference electrode), and the anodic limit on the Pt working electrode is -0.4 V (Fig. 2b) corresponding to oxygen evolution. The electrochemical window of molten $\text{Na}_2\text{CO}_3\text{-K}_2\text{CO}_3$ is 2.4 V which is obtained by the potential difference between anodic and cathodic limits. The electrochemical window obtained by CV is

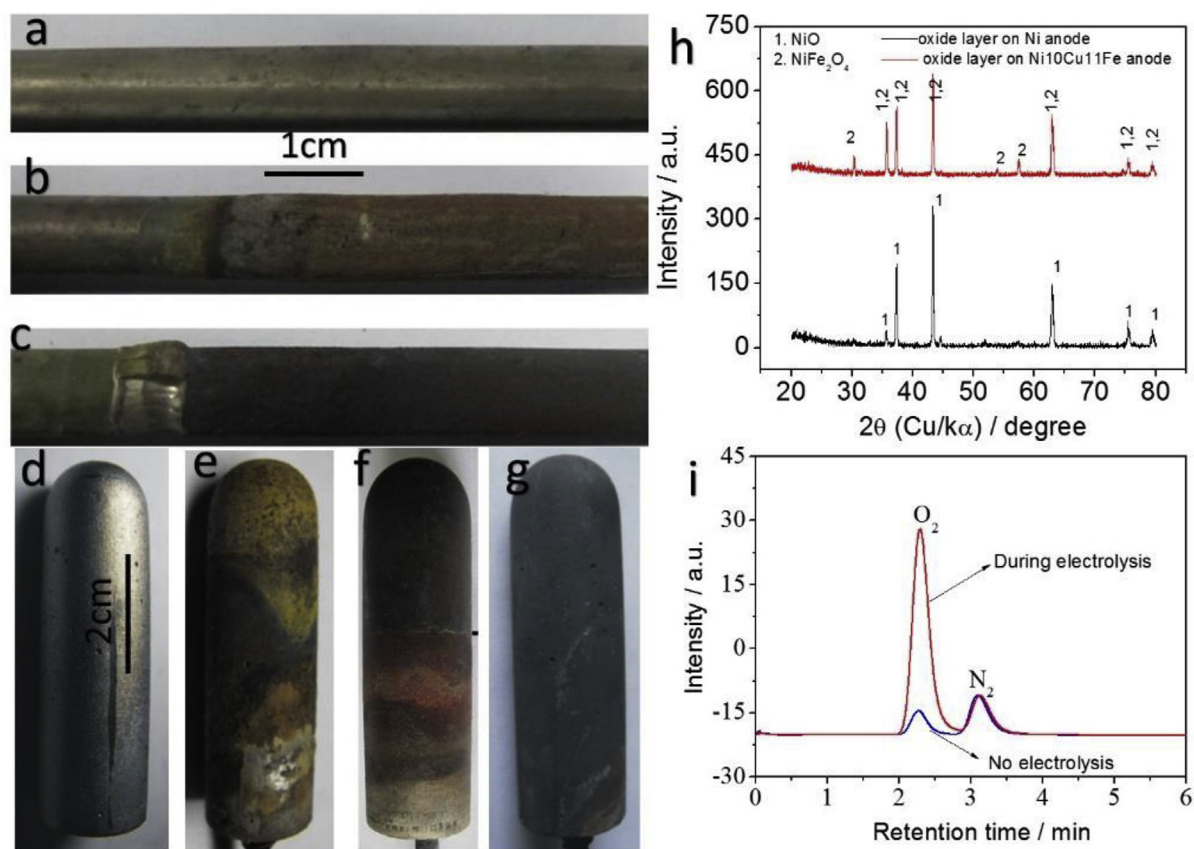


Fig. 3. (a–g) Images of nickel rod served as anode before (a) and after for 3 h (b) and 20 h (c), and Ni10Cu11Fe rod before (d) and after served as anode for 5 h (e), 12 h (f) and 150 h (g). (h) XRD patterns of the oxide layers from the Ni and Ni10Cu11Fe. (i) Gas chromatography spectrum of the outlet gas before and during electrolysis using the Ni10Cu11Fe anode.

only 0.06 V higher than that calculated by thermodynamic data, which may be due to the overpotential or lower oxygen pressure less than 1 atm. For the Ni electrode, obvious oxidation starts at -0.15 V. As the potential is polarized to -0.43 V, a significant current increase is due to the oxygen evolution which is in line with the Pt electrode. In the second scan, oxidation of Ni is negligible because a NiO layer has formed in the first scan, indicating the pre-formed NiO layer is a good electronic conductor because no substantial rise in overpotential for oxygen evolution was observed in the second and third scans. For the copper electrode (Fig. 2d), the oxidation starts at -0.1 V, and two oxidation peaks should be related to the formation of Cu₂O and CuO. In the second and third scan, a small oxidation peak still exists, indicating that the pre-formed oxide layer is porous. For the iron working electrode (Fig. 2e), two anodic peaks should correspond to the formation of FeO and Fe₂O₃/Fe₃O₄. For the Ni10Cu11Fe alloy working electrode, significant oxidation peak was observed prior to the oxygen evolution on the first cycle (Fig. 2f). No distinguishable oxidation peaks suggest that alloy exhibits different oxidation behaviors from that of the pure Ni, Cu and Fe. As the scanning cycle increases, the oxidation peak becomes smaller and smaller and finally reaches a stable state after ten cycles, suggesting that the oxidation film becomes denser and denser but without causing higher overpotential for oxygen evolution. The growth of the protective layer and the possible reactions that occurred in the oxide layer will be analyzed and discussed later.

3.3. Anode products analysis

Based on the results of CV, a pure Ni (diameter: 8 mm, Fig. 3a) and a home-made Ni10Cu11Fe rod (diameter: 20 mm, Fig. 3d) were respectively employed as anodes, coupling with an Fe₂O₃ cathode to test their stability and anodic products. Three hours later, a layer of khaki film was observed on the surface of Ni (Fig. 3b). The film was then confirmed to be NiO (Fig. 3h). A serious crack was observed at the gas/electrolyte interface of the Ni anode after 20 h (Fig. 3c), indicating that the formed NiO layer is not mechanically robust. In spite of the crack, the NiO does not dissolve in the molten salt, implying that the NiO is a stable layer to protect metals except for its fragility.

Then the Ni10Cu11Fe was employed as an anode in molten Na₂CO₃-K₂CO₃ to test its performance. After 5 h, the metallic shining alloy (Fig. 3d) became grey and partially yellowish (Fig. 3e). As the electrolysis duration increased to 12 h, the anode part immersed in the melt became grey (Fig. 3f). A uniform and smooth coating formed on the surface of the Ni10Cu11Fe after 150 h (Fig. 3g). The electrolyte/gas interface at the anode disappears as the increase of electrolysis duration, demonstrating that the Ni10Cu11Fe is quite stable. The grey layer on the surface of the Ni10Cu11Fe anode consists of NiO and NiFe₂O₄ (Fig. 3h). Thus, NiFe₂O₄ undoubtedly leads to the mechanical robustness of the oxide layer. Moreover, NiFe₂O₄ has been demonstrated to be an excellent inert anode material in molten salt [16,17]. Along with the unchanged dimension of the anode, the oxygen gas was collected

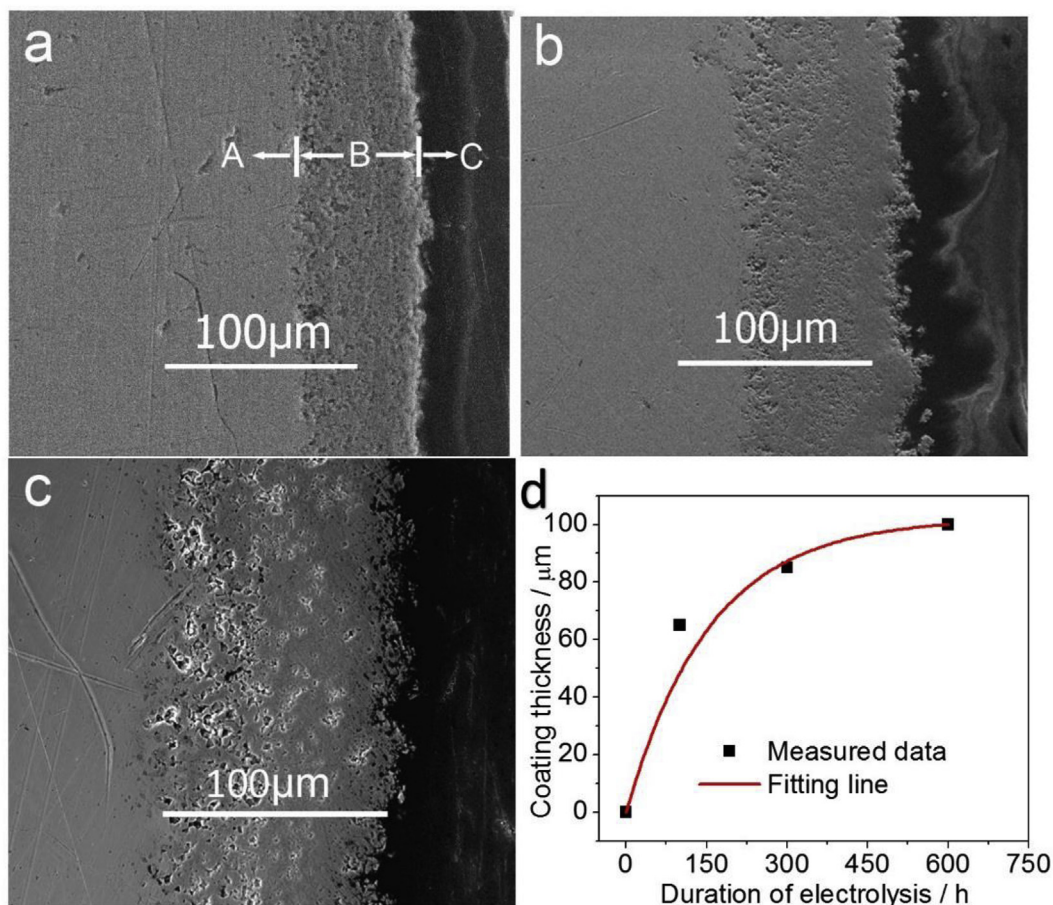


Fig. 4. (a–c) Cross-sectional SEM images of the Ni10Cu11Fe anode after 100 h (a), 200 h (b) and 600 h (c) electrolysis, area A, B, C are respectively denoted as the bulk metal, oxide layer and epoxy layer. (d) The profile of the thickness of oxide layer with the electrolysis duration.

by a GC instrument (Fig. 3i), further confirming the Ni10Cu11Fe is an inert anode capable of producing oxygen.

3.4. Analysis of the *in situ* formed oxide scale

The structures and compositions of the oxide scale are crucial to interpreting the function of the inert anode. As shown in Fig. 4a–c, a robust oxide layer grew on the surface of the alloy anode, and the thickness of the oxide layer increases with increasing electrolysis duration. A 65-μm-thick oxide layer formed after 100 h electrolysis, and the thickness of the layer grows to 85 and 100 μm after 200 h and 600 h, respectively.

As shown in Fig. 4d, the growth rate of the oxide layer tends to be slower with increasing electrolysis duration. After 600 h, the growth rate becomes very slow and the thickness of the oxide layer with time can be expressed as follow

$$L = 102.2 \times \left(1 - \exp\left(\frac{-t}{156}\right) \right) \quad (1)$$

where L is the thickness (μm), and t is the duration of the electrolysis (h). According to Eqn (1), the estimated maximum thickness of the oxide coating should be less than 102.2 μm. In general, the growth of the oxide film takes place at the interface of metal/

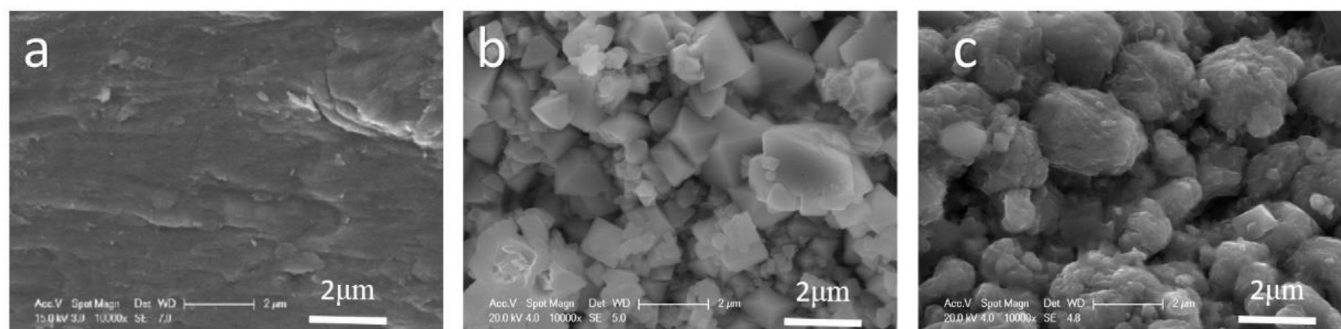


Fig. 5. SEM images of the surface of bare Ni10Cu11Fe (a) the inner side of the layer (after serving for 600 h) (b) and the outer side contacting the electrolyte (c).

oxide, and growth rate of the oxide film depends on the diffusion rate of oxygen ion in the oxide layer and the metal out from the bulk alloy [27–29]. At the beginning, a porous oxide layer allows oxygen penetration with consequent reaction with the alloy. As the electrolysis proceeds, not only does the thickness of the oxide layer increase, but also other reactions among the oxide layer and metal take place to make a denser layer, resulting in a long path and slow diffusion rate for oxygen ions. As a consequence, the growth rate of the oxide layer is minimized or, ideally, becomes zero, forming a desired coating for a metallic inert anode. According to the SEM image (Fig. 4a–c), the outermost layer seems to become denser and denser, leading to a better layer for blocking oxygen. The

microstructure of the Ni10Cu11Fe has been reported by Cheng et al. [26]. Before anodization, the surface of the alloy is quite smooth (Fig. 5a). A typical spinel structure was detected from the inner side of the oxide layer (Fig. 5b) and it should correspond to NiFe_2O_4 which has been confirmed by XRD observation. On the other surface of the layer, no typical crystalline structure, or sharp edge, was observed (Fig. 5c), but some particles with smoother surface were found because this surface directly contacted the electrolyte and was used for oxygen evolution. Importantly, both surfaces of the oxide layer are dense, favoring a good barrier to block oxygen.

The structure and element distribution were analyzed in more detail by SEM (backscattered electron imaging) and elemental

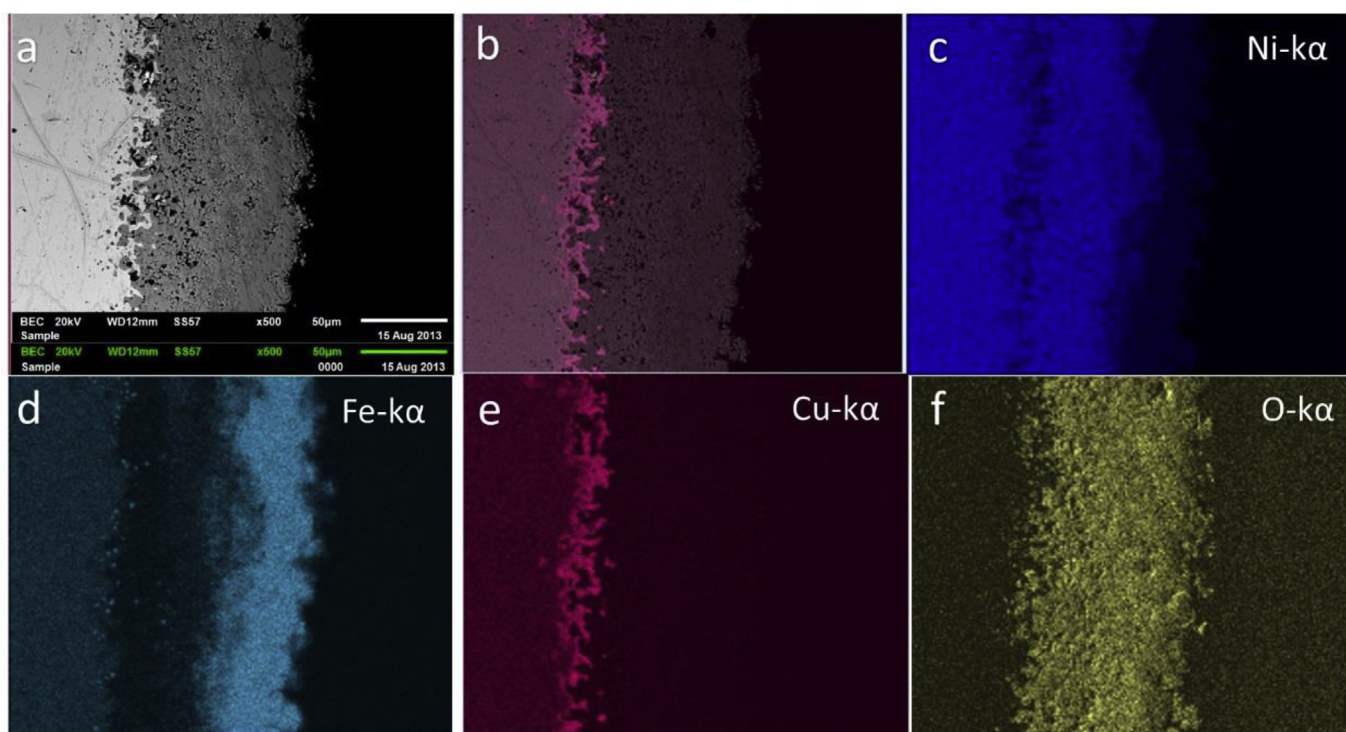


Fig. 6. (a) SEM image (backscattered electron imaging), overlap image of SEM image and elemental distribution mapping (b), (c–f) the elemental distribution maps of the Ni10Cu11Fe served as an anode for 600 h.

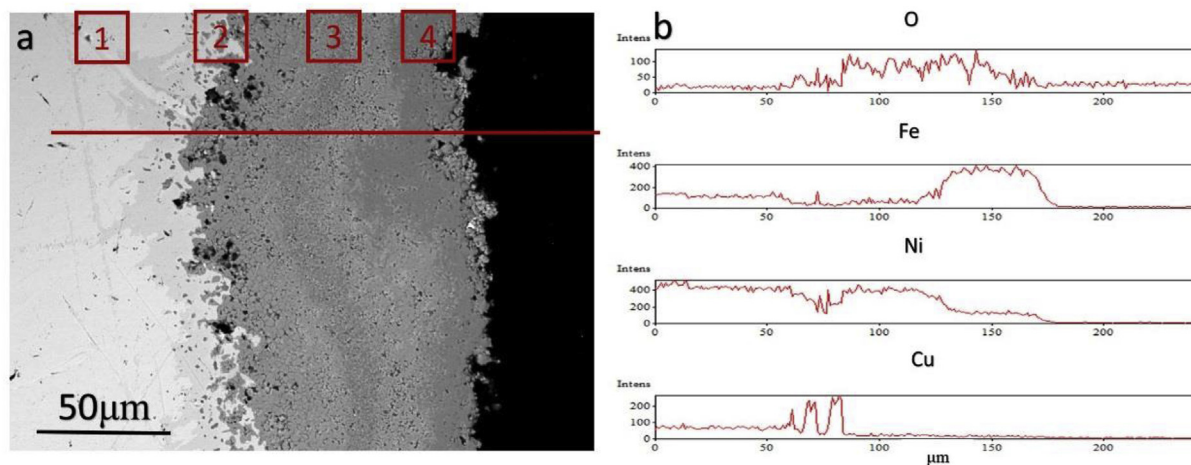


Fig. 7. (a) SEM images of the cross section of Ni10Cu11Fe served as an anode for 600 h, and (b) EDS linear analysis across the oxides layer (red line in a). (For interpretation of the references to colour in this figure legend, the reader is referred to the Web version of this article.)

mapping analysis (Fig. 6a–f). The oxide layer can be divided into three regions, from the inner to outer, which are denoted as Cu-rich region, Ni-rich region and Fe-rich region. Note that the Fe rich region is the densest layer which is advantageous for blocking oxygen. It is also of great interest to know compositions of each region and how Ni, Fe and Cu are separated in the oxide layer.

Chemical composition of the selected areas was quantitatively tested by EDS (Fig. 7 and Table 1). The composition of the bulk metal denoted as area-1 (Fig. 7a) matches the experimentally designed composition (note that the oxygen is hard to quantitatively measure by EDS). Area-2 covering the interface of metal/oxide shows a higher concentration of Cu but a lower concentration of Fe and Ni comparing with the primitive composition of the bulk Ni₁₀Cu₁₁Fe alloy. In the middle of the oxide layer, area-3, oxygen concentration remarkably increases while copper concentration dramatically drops and iron concentration increases a little compared to area-2. The outside of the oxide layer, area-4, contains the highest iron concentration, and the copper concentration is still low while the Ni concentration decreases. Note that the atomic ratio of Fe and Ni in area-4 is close to 2 (Table 1), along with the XRD analysis, confirming that the dense outside layer is NiFe₂O₄. In the middle the oxide layer, NiO is a dominating compound with a small amount of NiFe₂O₄. A thin copper-rich layer lies between the bulk metal and NiO layer. Overall, a three-layer coating (Cu/NiO/NiFe₂O₄) is *in-situ* formed to protect the alloy anode and enable oxygen evolution. As shown in Fig. 7b, the thicknesses of the Cu, NiO and NiFe₂O₄ layers are ~20 μm, ~50 μm, and ~30 μm, respectively. More detailed information about the growing process and mechanism of different layers need more efforts in the future.

The electrical conductivity is another important criterion for selecting alloy anode with an oxide coating. EIS measurements were conducted to measure the resistance of the Ni₁₀Cu₁₁Fe anode in molten Na₂CO₃-K₂CO₃ at 750 °C. Before electrolysis, the overall resistance of the anode and electrolyte is about 0.024 Ω cm². After 100 h electrolysis, the overall resistance of the anode, oxide layer and electrolyte is about 0.045 Ω cm², illustrating that the increase of 0.021 Ω cm² is due to the oxide layer formed on the anode. After 300 h and 600 h, the resistance increases to 0.051 Ω cm² and 0.054 Ω cm², respectively, corresponding to the resistance of the oxides layer of 0.027 Ω cm² (300 h) and 0.03 Ω cm² (600 h) (assuming the resistance of the alloy is constant during electrolysis). Together with the thickness and surface area of the anode, the electrical conductivities of the oxide layer obtained for 100, 200 and 600 h are 0.22, 0.17 and 0.15 S cm⁻¹, which are calculated by Ohm's Law (the surface area is ~15 cm² and thickness of the layer is obtained from SEM images). The electrical conductivity of the oxide coating is close to that of pure NiFe₂O₄ reported by Liu et al. [18], further confirming that the oxide coating will not result in high internal resistance voltage drop. The overall resistance of the anode with a 100-μm-thick oxide coating is 0.03 Ω cm² and the resistance varies linearly with the thickness of the oxide coating (Fig. 8). The expected maximum thickness of the oxide coating is ~102 μm, corresponding to a maximum resistance of ~0.0308 Ω cm². Since the boundaries of the multi-layers cannot be accurately distinguished, the contribution of the resistance from each layer of the scale is not given here.

Table 1
Elemental analysis of selected areas in Fig. 7.

Atomic ratio	Bulk metal (1)	Layer 1 (2)	Layer 2 (3)	Layer 3 (4)
Ni	76.8	72.2	59.7	23
Fe	10	3.3	5	48
Cu	10.6	20.4	0.4	0.4
O	2.6	4	34.9	28.7

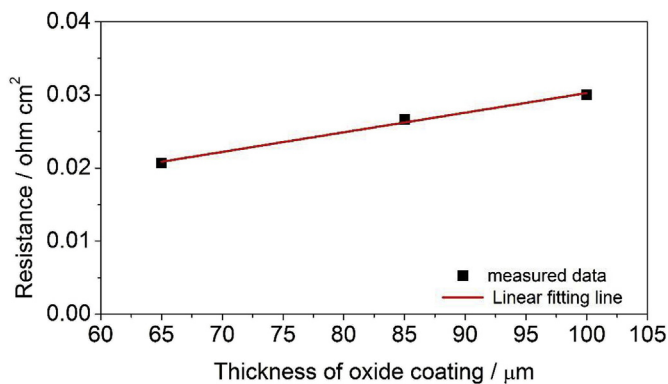


Fig. 8. Resistance of an anode with oxide scale of different thicknesses.

The schematic of the three-layer scale coated Ni₁₀Cu₁₁Fe anode is shown in Fig. 9. To understand the mechanism of forming the three-layer coating is worthwhile for designing and screening materials for inert anode development. The formation of the three-layered structure should involve the process of element diffusion and separation, and the driving force of the diffusion and/or migration correlates to the chemical and/or electrochemical reactions happening at the interfaces and inside of the oxide layers. At the very beginning of the electrolysis, all Ni, Fe and Cu will be oxidized together, generating the oxide layer and metal/oxides interface. Because the anode was constantly polarized to enable oxygen evolution, the oxides at the outmost surface should be at the highest oxidation state. Beneath the surface oxide layer, a compounding reaction, like Fe₂O₃ reacting with NiO to form a more stable NiFe₂O₄ occurs. At the interface of the metal/oxides, a displacement reaction spontaneously takes place. As the Fe is the most reactive metal in the alloy, Fe will diffuse out from the alloy to displace Ni and Cu from NiO and CuO/Cu₂O, resulting in the outward diffusion of Fe and inward diffusion of Ni and Cu [30–33]. As the electrolysis proceeds, the oxide layer continuously grows and gradually forms a three-layered structure. When the oxide is thick and dense enough to prevent oxygen ion from reacting with the

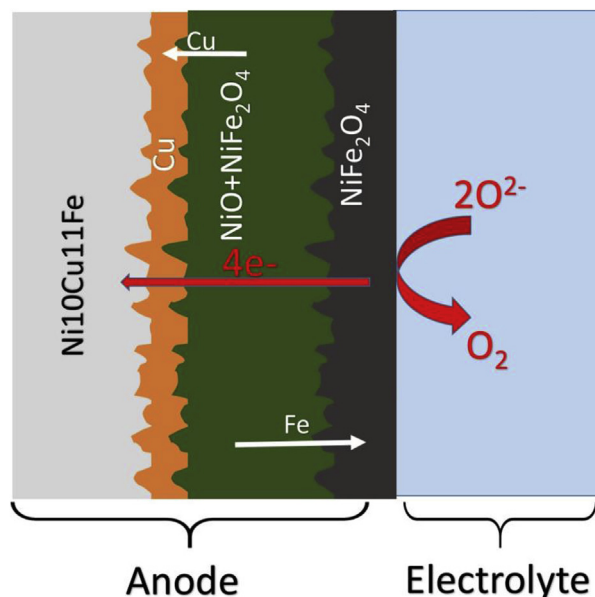


Fig. 9. Schematic of the three-layer scale coated Ni₁₀Cu₁₁Fe anode.

bare metal, a stable oxide layer functions as a protecting layer and enables oxygen evolution. In a word, the dense outer NiFe_2O_4 layer is used for oxygen evolution and electrolyte permeation inside, while the middle NiO layer conducts electrons and blocks the oxygen ions together, as does the NiFe_2O_4 layer. The copper-rich layer could decrease the oxygen pressure inside the scale, resulting in reducing the driving force for the generation of iron- and Ni-oxides and thereby slowing down the growth rate of the oxide scale.

4. Conclusions

The Ni10Cu11Fe alloy was proved to be a cost-effective and long-lasting inert anode in a Na_2CO_3 - K_2CO_3 eutectic melt, producing oxygen and extracting metals from oxide precursors without greenhouse and toxic gas emissions. Three layers, from the inside to outside, are, respectively, Cu, NiO, and NiFe_2O_4 , formed on the surface of the Ni10Cu11Fe anode. This anode protected by an *in situ* formed three-layered coating is able to survive in molten carbonate for more than 600 h. This three-layered structure, first revealed here, is key to the excellent performances of the anode. Moreover, the multilayer-structure coating could also be employed for developing low-cost alloy inert anodes for other high-temperature electrolysis cells, such as the Hall-Héroult cell, and this electrochemical oxidation approach in molten carbonates could be used for surface engineering at high temperatures.

Acknowledgments

The authors gratefully acknowledge financial support from NSFC (51325102, 21673162), MOST (2015DFA90750) and the Nature Science Foundation of Hubei Province of China (Team Project, 2015CFA017).

References

- [1] I. Galasiu, R. Galasiu, Aluminium electrolysis with inert anodes and wettable cathodes and with low energy consumption, in: M. Gaune-Escard, G.M. Haarberg (Eds.), *Molten Salts Chemistry and Technology*, John Wiley & Sons, Ltd, 2014, pp. 27–37.
- [2] S. Helle, M. Pedron, B. Assouli, B. Davis, D. Guay, L. Roué, Structure and high-temperature oxidation behaviour of Cu–Ni–Fe alloys prepared by high-energy ball milling for application as inert anodes in aluminium electrolysis, *Corros. Sci.* 52 (2010) 3348–3355.
- [3] G.Z. Chen, D.J. Fray, T.W. Farthing, Direct electrochemical reduction of titanium dioxide to titanium in molten calcium chloride, *Nature* 407 (2000) 361–364.
- [4] A.M. Abdelkader, K.T. Kilby, A. Cox, D.J. Fray, DC voltammetry of electro-deoxidation of solid oxides, *Chem. Rev.* 113 (2013) 2863–2866.
- [5] W. Xiao, D.H. Wang, The electrochemical reduction processes of solid compounds in high temperature molten salts, *Chem. Soc. Rev.* 43 (2014) 3215–3228.
- [6] A. Allanore, Electrochemical engineering of anodic oxygen evolution in molten oxides, *Electrochim. Acta* 110 (2013) 587–592.
- [7] A. Allanore, L. Yin, D.R. Sadoway, A new anode material for oxygen evolution in molten oxide electrolysis, *Nature* 497 (2013) 353–356.
- [8] A.H. Caldwell, E. Lai, A.J. Gmitter, A. Allanore, Influence of mass transfer and electrolyte composition on anodic oxygen evolution in molten oxides, *Electrochim. Acta* 219 (2016) 178–186.
- [9] H.Y. Yin, X.H. Mao, D.Y. Tang, W. Xiao, L. Xing, H. Zhu, D.H. Wang, D.R. Sadoway, Capture and electrochemical conversion of CO_2 to value-added carbon and oxygen by molten salt electrolysis, *Energy Environ. Sci.* 6 (2013) 1538–1545.
- [10] H.Y. Yin, D.Y. Tang, H. Zhu, Y. Zhang, D.H. Wang, Production of iron and oxygen in molten K_2CO_3 - Na_2CO_3 by electrochemically splitting Fe_2O_3 using a cost affordable inert anode, *Electrochem. Commun.* 13 (2011) 1521–1524.
- [11] K.F. Du, K.Y. Zheng, Z.G. Chen, H. Zhu, F.X. Gan, D.H. Wang, Unusual temperature effect on the stability of nickel anodes in molten carbonates, *Electrochim. Acta* 245 (2017) 402–408.
- [12] D.Y. Tang, H.Y. Yin, X.H. Cheng, W. Xiao, D.H. Wang, Green production of nickel powder by electro-reduction of NiO in molten Na_2CO_3 - K_2CO_3 , *Int. J. Hydrogen Energy* 41 (2016) 18699–18705.
- [13] D.R. Sadoway, Inert anodes for the Hall-Héroult cell: the ultimate materials challenge, *JOM-J. Miner. Met. Mater. Soc.* 53 (2001) 34–35.
- [14] E. Olsen, J. Thonstad, Nickel ferrite as inert anodes in aluminium electrolysis: Part I - material fabrication and preliminary testing, *J. Appl. Electrochem.* 29 (1999) 293–299.
- [15] E. Olsen, J. Thonstad, Nickel ferrite as inert anodes in aluminium electrolysis: Part II - material performance and long-term testing, *J. Appl. Electrochem.* 29 (1999) 301–311.
- [16] L. Ma, K. Zhou, Z. Li, Hot corrosion of a novel (Ni,Co)O/(Ni,Co) Fe_2O_4 composite coating thermally converted from an electrodeposited Ni–Co– Fe_2O_3 composite coating, *Corros. Sci.* 53 (2011) 2357–2367.
- [17] L. Ma, K. Zhou, Z. Li, Q. Wei, L. Zhang, Hot corrosion of a novel NiO/Ni Fe_2O_4 composite coating thermally converted from the electroplated Ni–Fe alloy, *Corros. Sci.* 53 (2011) 3712–3724.
- [18] B.G. Liu, L. Zhang, K.C. Zhou, Z.Y. Li, H. Wang, Electrical conductivity and molten salt corrosion behavior of spinel nickel ferrite, *Solid State Sci.* 13 (2011) 1483–1487.
- [19] V. Chapman, Barry J. Welch, M. Skyllas-Kazacos, High temperature oxidation behaviour of Ni–Fe–Co anodes for aluminium electrolysis, *Corros. Sci.* 53 (2011) 2815–2825.
- [20] J.A. Sekhar, J. Liu, H. Deng, J.J. Duruz, V. de Nora, in: B.J. Welch (Ed.), *Light Metals 1998*, vols. 597–603, Minerals, Metals & Materials Soc, Warrendale, 1998.
- [21] E. Gavrilova, G. Goupil, B. Davis, D. Guay, L. Roué, On the key role of Cu on the oxidation behavior of Cu–Ni–Fe based anodes for Al electrolysis, *Corros. Sci.* 101 (2015) 105–113.
- [22] G. Goupil, S. Jucken, D. Poirier, J.G. Legoux, E. Irissou, B. Davis, D. Guay, L. Roué, Cold sprayed Cu–Ni–Fe anode for Al production, *Corros. Sci.* 90 (2015) 259–265.
- [23] I. Galasiu, R. Galasiu, J. Thonstad, Inert Anode for Aluminum Electrolysis, first ed., Aluminum-Verlag Marketing & Kommunikation GmbH, 2007.
- [24] I. Gallino, M.E. Kassner, R. Busch, Oxidation and corrosion of highly alloyed Cu–Fe–Ni as inert anode material for aluminum electrowinning in as-cast and homogenized conditions, *Corros. Sci.* 63 (2012) 293–303.
- [25] K.L. Van, K. Le Van, H. Groult, F. Lantelme, M. Dubois, D. Avignant, A. Tressaud, S. Sigrist, Electrochemical formation of carbon nano-powders with various porosities in molten alkali carbonates, *Electrochim. Acta* 54 (2009) 4566–4573.
- [26] X.H. Cheng, L. Fan, H.Y. Yin, L. Liu, K.F. Du, D.H. Wang, High-temperature oxidation behavior of Ni-11Fe-10Cu alloy: growth of a protective oxide scale, *Corros. Sci.* 112 (2016) 54–62.
- [27] O. Kubaschewski, B.E. Hopkins, *Oxidation of Metals and Alloys*, second ed., Academic Press, Butterworths, 1962. London.
- [28] C. Honvault, V. Peres, L. Cassayre, P. Chamelot, P. Palau, S. Bouvet, M. Pijolat, Oxidation kinetics of a Ni–Cu based cermet at high temperature, *Corros. Sci.* 68 (2013) 154–161.
- [29] R.T. Foley, Oxidation of iron-nickel alloys VI. A survey of kinetics and mechanism, *J. Electrochem. Soc.* 109 (1962) 1202–1206.
- [30] Y.P. Zhu, Y.D. He, D.R. Wang, Fe-30Ni-5NiO alloy as inert anode for low-temperature aluminum electrolysis, *JOM-J. Miner. Met. Mater. Soc.* 63 (2011) 45–49.
- [31] G. Goupil, G. Bonnefont, H. Idrissi, D. Guay, L. Roué, Consolidation of mechanically alloyed Cu–Ni–Fe material by spark plasma sintering and evaluation as inert anode for aluminum electrolysis, *J. Alloys Compd.* 580 (2013) 256–261.
- [32] S. Helle, B. Brodu, B. Davis, D. Guay, L. Roué, Influence of the iron content in Cu–Ni based inert anodes on their corrosion resistance for aluminium electrolysis, *Corros. Sci.* 53 (2011) 3248–3253.
- [33] S. Helle, M. Tresse, B. Davis, D. Guay, L. Roué, Mechanically alloyed Cu–Ni–Fe–O based materials as oxygen-evolving anodes for aluminum electrolysis, *J. Electrochem. Soc.* 159 (2012) E62–E68.